JACS
JOURNAL OF THE AMERICAN CHEMICAL SOCIETY

COMMUNICATION

pubs.acs.org/JACS

Efficient Synthesis of Highly Luminescent Copper Indium Sulfide-Based Core/Shell Nanocrystals with Surprisingly Long-Lived Emission

Liang Li, Anshu Pandey, Donald J. Werder, Bishnu P. Khanal, Jeffrey M. Pietryga, and Victor I. Klimov*

Center for Advanced Solar Photophysics, *C-PCS*, Chemistry Division, Los Alamos National Laboratory, Los Alamos, New Mexico 87545, United States

Supporting Information

ABSTRACT: We report an efficient synthesis of copper indium sulfide nanocrystals with strong photoluminescence in the visible to near-infrared. This method can produce gram quantities of material with a chemical yield in excess of 90% with minimal solvent waste. The overgrowth of as-prepared nanocrystals with a few monolayers of CdS or ZnS increases the photoluminescence quantum efficiency to > 80%. On the basis of time-resolved spectroscopic studies of core/shell particles, we conclude that the emission is due to an optical transition that couples a quantized electron state to a localized hole state, which is most likely associated with an internal defect.

Recently, nanocrystals (NCs) of ternary compositions such as copper indium sulfide (CIS) have been gaining increased attention due to their wide range of potential applications. CIS and its heavier congener, copper indium selenide, have band gaps (1.5 and 1.05 eV, respectively) that are well suited for applications in thin-film photovoltaics (PVs) utilizing either bulk or NC forms of these materials.[1] Further, the emission of CIS NCs can be tuned from the visible into the near-infrared (near-IR) spectral ranges, making them relevant for applications in lighting and displays. Finally, these NCs are of interest in biolabeling, especially because recent studies have indicated that CIS NCs have markedly lower toxicity than cadmium-based NCs.[2]

The synthesis of CIS NCs has evolved from early methods involving treatment of aqueous Cu(I) and In(III) with a saturated hydrogen sulfide solution[3] to techniques including solvothermal synthesis,[4] thermolysis,[5] photochemical decomposition,[6] and the hot-injection method.[7] Recently, synthetic methods have also been developed for controlling the crystal structure of the NCs, specifically demonstrating that, by adjusting ligand composition, one can produce particles with either *tetragonal chalcopyrite* or *wurtzite* structures.[8]

Despite such progress, existing methods for fabricating high-quality CIS NCs are not well suited for the large-scale production needed for applications such as PVs or solid-state lighting, as they rely on fast precursor injection to induce nucleation and/or produce large amounts of waste solvent. Other factors that limit the applicability of these NCs include relatively low emission efficiencies (typically <30%, even after growth of a passivating shell) and a poor understanding of the mechanisms for both light emission and non-radiative carrier losses.

Here, we describe the synthesis of CIS NCs with high as-synthesized photoluminescence (PL) quantum yields (QYs) via a scalable reaction with very high chemical yields of ~90%. This method does not require precursor injection and relies on inexpensive reagents. A further advantage over other recent non-injection approaches[9] is the use of the anion precursor also *as both ligand and solvent*, which allows for nearly complete consumption of the more expensive cationic precursors, minimizes the number of reagents used in the synthesis, and produces minimal solvent waste. All of these features make this technique highly scalable and well suited for high-throughput production of CIS NCs. We also demonstrate that the overgrowth of CIS NCs with a few monolayers of CdS or ZnS significantly improves PL QYs up to more than 80%. Finally, we perform time-resolved spectroscopic studies aimed at elucidating the nature of both radiative and non-radiative recombination mechanisms. While as-synthesized CIS NCs show non-exponential PL dynamics, following overcoating, PL decay becomes almost purely exponential, which implies the existence of a single recombination channel across the entire NC ensemble.

In a typical synthesis of CIS NCs, indium acetate (0.292 g, 1 mmol) is mixed with copper(I) iodide (0.190 g, 1 mmol) and 1-dodecanethiol (DDT, 5 mL) in a three-necked flask. The reaction mixture is degassed under vacuum for 5 min and purged with argon three times. The flask is heated to 100 °C for 10 min until a clear solution is formed. The temperature is then raised to 230 °C. As the temperature increases, the color of the reaction solution progressively changes from colorless to green, yellow, red, and finally black, indicating nucleation and subsequent growth of CIS NCs. Figure 1a shows the absorption and emission spectra of a typical CIS sample. Over the course of 1 h, the PL peak shifts from 630 to 780 nm (Figure 1b), which can be correlated to an increase in particle size (Figure 1a inset), as determined by transmission electron microscopy (TEM). A corresponding shift is also observed in the absorption spectra. Use of a higher reaction temperature results in faster growth of the NCs, which we attribute to an increase in the DDT decomposition rate. At the desired size, the reaction is quenched by immersing the flask in a water bath. The product NCs can be isolated by precipitating by addition of acetone, centrifuging, and decanting the supernatant. The solid NC product is redispersible in hexane. In this synthesis, DDT acts as the sulfur precursor

Received: September 13, 2010
Published: January 5, 2011

dx.doi.org/10.1021/ja108261h | *J. Am. Chem. Soc.* 2011, 133, 1176–1179

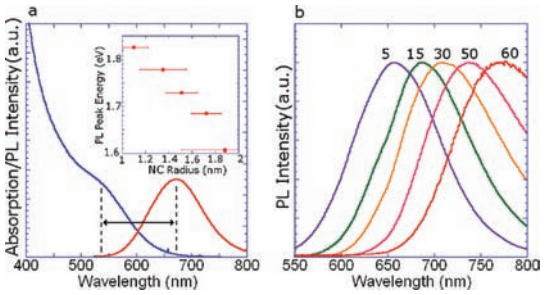

Figure 1. (a) Absorption and emission spectra of a sample of CIS NCs. The apparent ("global") Stokes shift (arrow) is 0.46 eV. Inset: PL peak energy as a function of NC size as determined by TEM. (b) Evolution of emission spectra during a typical synthesis. The numbers correspond to reaction time in minutes.

Table 1. Copper:Indium Ratios in CIS NCs of Various Sizes

growth time (min)	10	20	30
d (nm)[a]	2.2 ± 0.2	2.7 ± 0.2	3.3 ± 0.3
Cu:In (EDX)	0.96 ± 0.08	0.970 ± 0.03	1.07 ± 0.04

[a] Diameters determined by TEM.

as well as the solvent, thereby eliminating the use of additional solvents. Furthermore, the large excess of anionic precursor ensures nearly complete consumption of the cationic precursors, leading to an extremely high (~90%) chemical yield relative to the indium and copper reagents and a minimum of solvent waste. By scaling up the amounts of metal precursors 3-fold, *but without any additional DDT*, up to 0.8 g of CIS NCs was obtained from a single reaction.

TEM indicates that the NCs are tetrahedral, with a size dispersion typically around 10%. X-ray diffraction (XRD) studies support a tetragonal chalcopyrite structure. Energy-dispersive X-ray spectroscopy (EDX) reveals that the Cu:In ratio for all samples is close to the ideal 1:1, irrespective of growth time (Table 1). The strong dependence of the stoichiometry on reaction time observed in previous reports may be indicative of the formation of Cu interstitials that are typically produced under anion-deficient conditions.[10] The large excess of sulfur precursor that results from the use of DDT as solvent renders such conditions essentially impossible to achieve. Also based on EDX measurements, the Cu:S ratio in as-synthesized NCs is slightly greater than 1:2; the excess amount of sulfur can be attributed to the presence of thiol ligands on the NC surfaces.

The as-prepared NCs have good PL QYs of 5−10%, superior to those achieved in previous reports[7b,7c] and comparable to those of as-prepared CdSe NCs. To further improve PL efficiency, we use inorganic surface passivation with a shell of CdS or ZnS, both of which have a wider energy gap than CIS.

In the overcoating procedure, 1 mL of original NC growth solution is diluted with 4 mL of 1-octadecene (ODE) and then degassed three times. For adgrowth of a CdS (ZnS) shell, a mixture of 0.4 mmol of cadmium oleate (zinc stearate), 0.4 mmol of sulfur dissolved in trioctylphosphine (1 M solution), and 4 mL of ODE is added dropwise into the reaction solution at 210 °C over 20 min. Shell growth was confirmed by size analysis of TEM images and elemental analysis by EDX.

Following shell growth, the overall size of the particles increases, and they maintain a tetrahedral shape (Figure 2c,d).

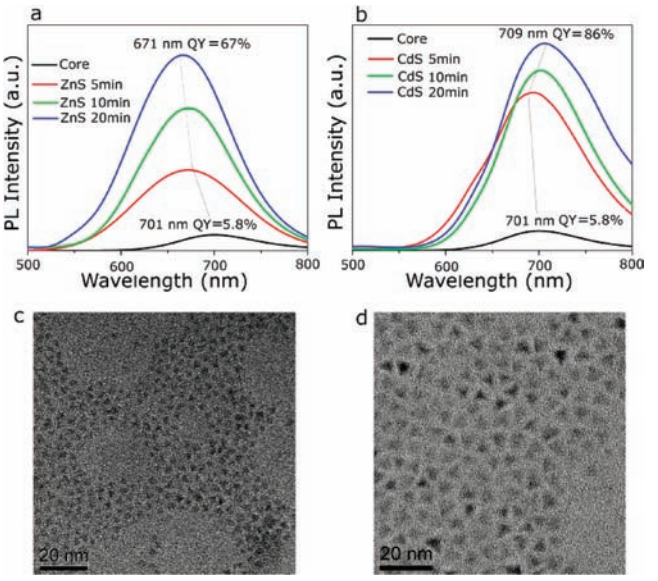

Figure 2. Evolution of the PL spectra of CIS NCs during the growth of (a) a ZnS shell and (b) a CdS shell. TEM images of (c) uncoated CIS NCs and (d) CIS/ZnS core/shell structures.

The overgrowth with ZnS typically leads to a blue shift of the PL spectrum (Figure 2a), which is likely indicative of etching of the core material under shell growth conditions and the associated increase in the degree of spatial confinement. CdS overgrowth proceeds with a similar initial blue shift, followed by a subsequent red shift; the latter is consistent with slight delocalization of the electron into the CdS layer (Figure 2b) due to the significantly lower-lying conduction band relative to that of ZnS.

The use of either ZnS or CdS overcoating results in a dramatic improvement of the PL quantum yield—up to 10-fold for ZnS and slightly higher still for CdS. CIS NCs with a single-monolayer shell of CdS routinely exhibit PL QYs of >60%, while the record value is as high as 86%. These NCs are markedly brighter than the 30% QY CIS NCs recently reported by Xie et al.[7b] In another literature example, Li et al.[11] described CIS NCs with PL QYs up to 60%; however, these NCs exhibited multi-featured PL spectra that may suggest structural inhomogeneity. In contrast, our highly emissive NCs are characterized by a single, well-defined emission band with a position that can be accurately controlled by growth conditions and strongly correlated to NC size.

To understand the mechanism underlying the dramatic improvement in emission efficiency in core/shell particles, we studied the PL dynamics of the CIS NCs before and after shell growth. In these measurements, samples were excited at 400 nm by 250 fs pulses at 250 kHz repetition rate, and PL was detected using spectrally resolved, time-correlated single photon counting (1 ns time resolution).

We observe that the PL decay is not single-exponential in as-prepared CIS NC samples (Figure 3a). Further, the PL dynamics are spectrally non-uniform and are significantly faster on the blue side of the emission band (a few nanoseconds time constant) than on its red side (hundreds of nanoseconds decay constant; Figure 3a inset). For all samples, a sum of two exponentials (time constants of 6.5 and 190 ns for the sample in Figure 3a) describes PL decay very well across the entire emission profile, with variations in amplitude accounting for the observed spectral dependence of

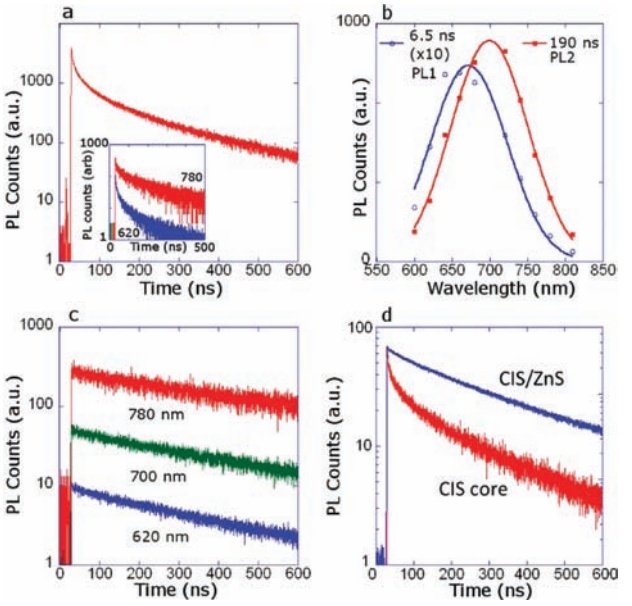

Figure 3. (a) Spectrally integrated PL relaxation for CIS NCs is biexponential with constants 6.5 and 190 ns that dominate emission decay on the blue (620 nm) and the red (780 nm) sides of the PL band, respectively (inset). (b) On the basis of a double-exponential analysis, the PL spectrum can be decomposed into fast (open blue circles) and slow (solid red squares) components centered at 670 and 700 nm, respectively. (c) Overcoating the core with a CdS layer eliminates the fast decay channel and results in spectrally uniform single-exponential decay with a 500 ns time constant. (d) Overcoating with ZnS also greatly reduces the contribution from the fast decay channel (spectrally integrated PL).

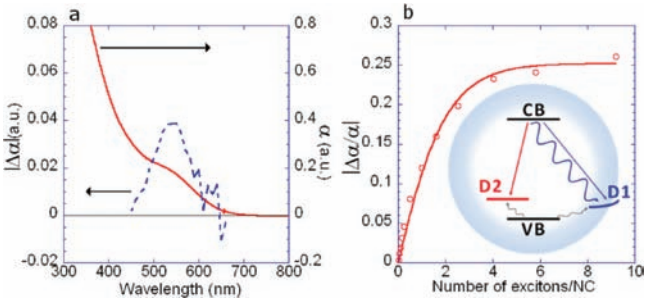

Figure 4. (a) TA spectrum ($\Delta\alpha$ is the pump-induced change in the absorption coefficient α) of a typical CIS/CdS sample shows a bleach feature (dashed) located near the band-edge absorption feature (solid); pump fluence is 4 mJ cm^{-2} at 400 nm; pump−probe delay time is 4 ps. (b) Bleach amplitude as a function of the average NC occupancy (symbols). The line represents a Poisson fit. Inset: The two recombination pathways observed in CIS NCs involve an electron in the quantized conduction band (CB) state and a hole trapped at either a surface defect (D1, blue) or an internal defect (D2, red). In core/shell NCs, D1 is eliminated, and overall relaxation becomes dominated by the slower D2-based channel. Straight and wavy arrows show radiative and nonradiative relaxation pathways, respectively.

the total decay rate. This biexponential analysis indicates that the short-lived contribution to the PL signal is associated with a higher energy band at 670 nm (PL1), while the longer-lived signal is due to a lower-energy band at 700 nm (PL2, Figure 3b).

Interestingly, overcoating with CdS completely eliminates the fast PL component and results in uniform single-exponential decay across the whole emission profile (Figure 3d), which can be correlated to the dramatic growth in emission QY. In the example in Figure 3, it increases from 5.8% for the core-only sample to 86% in the core/shell structure. This behavior, indicative of a single highly emissive recombination channel across the entire NC ensemble, is very unusual and rarely observed, even in the highest-quality CdSe NCs. Overcoating with ZnS also improves PL QYs relative to core particles; however, the PL dynamics still retain some biexponential character, which indicates some residual presence of the second recombination pathway with a poorer emission yield (Figure 3d).

Our observations that surface treatment suppresses a faster decay channel and simultaneously improves PL efficiency suggest that this channel is associated with recombination through a surface defect, which serves primarily as a center for non-radiative decay. The fact that the highly emissive channel that dominates carrier decay following shell growth is extremely slow (500 ns for sample in Figure 3c) is somewhat surprising. On the basis of the dielectric constants of bulk CIS,[12] the absorption cross section of CIS NCs at 400 nm is expected to be $(\sim 1.8 \times 10^{-16})a^3$ (cm^2), where a is the particle radius in nm and a refractive index of 1.45 has been assumed for the solvent. This is similar to the cross section of CdSe NCs, $(\sim 3 \times 10^{-16})a^3$ (cm^2).[13] Based on these numbers, the oscillator strength of the band-edge emitting transition in CIS NCs is estimated to be similar to that in CdSe NCs, which should result in similar radiative lifetimes. However, room-temperature exciton lifetime in CdSe NCs is 15−30 ns,[14] more than an order of magnitude shorter than we observe for CIS/CdS NCs. Long PL decay components in the CIS NC emission band have been previously attributed to surface traps;[9,15] however, our observation of increased PL lifetimes with improved surface passivation contradicts such an assignment.

To further probe the nature of CIS NC emission, we performed transient absorption (TA) studies. In TA measurements, the NCs were excited at 1 kHz repetition rate by frequency-doubled (400 nm), 150 fs pulses derived from an amplified Ti:sapphire laser. The pump-induced absorption changes were probed using variably delayed pulses of a femtosecond white-light continuum.

Optical excitation of CIS/CdS core/shell NCs results in a pronounced bleaching feature at band-edge spectral energies (Figure 4a). A similar feature is also seen for uncoated CIS NCs. In the example in Figure 4a, the bleach develops at the position of the band-edge absorption feature, about 0.4 eV to the blue from the PL peak. This observation implies that the large "global" Stokes shift between the emission line and the band-edge absorption is not due to strong electron−phonon coupling (i.e., a large Huang−Rhys factor) but is rather indicative of the involvement of intra-gap trap sites in the emission process. This conclusion is further supported by our observation that, in the case of larger CIS samples, the low-energy tail of the PL band extends below the bulk CIS band-edge.

We observe that the bleach feature saturates at higher fluences, indicating a finite degeneracy of electronic states involved in the band-edge transition (Figure 4b). The average NC occupancy for a given fluence was determined using an NC absorption cross section of $\sim 5 \times 10^{-16}$ cm^2, estimated on the basis of the mean NC radius of 1.4 nm (derived from TEM studies). The TA data can be accurately described using Poisson statistics of photon absorption events and assuming that the band-edge state responsible for TA saturation has a two-fold degeneracy; hence, multiexcitons of order two and higher contribute equally to the

dx.doi.org/10.1021/ja108261h |J. Am. Chem. Soc. 2011, 133, 1176–1179

band-edge bleach.[13] Given that CIS has a three-fold degenerate valence band structure, a higher-level of degeneracy is expected for holes; therefore, we assign the "saturable" two-fold degenerate level to the electron. This leads to the conclusion that the localized carrier must be the hole. Thus, the band-edge bleach is solely due to state filling associated with electrons in the lowest-energy quantized state without a discernible contribution from holes. A similar situation has been previously observed in CdSe NCs, where the strong band-edge bleach is dominated by the population of the lowest energy 1S electron level.[16]

As stated above, uncoated CIS particles show the same bleach behavior as core/shell particles. At the same time, both the "fast" and the "slow" emission bands in bare particles experience similar energy shifts with increasing particle radius. From this observation, we can infer that both decay channels involve the same quantized electron level but, to account for their energy difference, two different hole trap sites. The first channel (D1 trap in the inset of Figure 4b) produces fast, primarily non-radiative decay that is largely eliminated by shell growth and so can be associated with a surface state. The other channel (associated with the D2 trap; Figure 4b inset) results in slow, highly emissive decay. The second channel is not affected by shell growth, meaning that it must stem from an internal defect state, such as a substitutional defect in which the I and III ions are swapped.[17]

A very long PL lifetime observed for core/shell NCs is consistent with an emissive transition involving an extended electron quantized state and a localized hole state. This situation would be characterized by a large disparity in localization volumes of the electron and the hole and thus a reduced spatial overlap of their wave functions that would lead to slowed radiative decay.

To conclude, we have reported a new, highly scalable, "waste-free" synthesis of CIS NCs, which is characterized by a ca. 90% chemical yield. Using inorganic passivation with CdS or ZnS, we can improve PL QYs from 5−10% in as-prepared NCs to more than 80% for a core/shell structure, an increase that can be attributed to suppression of a fast, primarily non-radiative recombination process associated with surface-related traps. Parallel studies of core and core/shell particles reveal an extremely long radiative lifetime of ca. 500 ns. The long emission lifetime and the large "global" Stokes shift between the PL band and the band-edge absorption feature, coupled with the observation of a pronounced NC size-dependence of emission wavelength, are inconsistent with either strictly band-edge recombination or recombination between two localized states. Instead, they indicate that the radiative recombination in these NCs involves a transition from a quantized conduction-band state to a localized intra-gap state, which can be either a surface defect or an internal defect (e.g., of a substitutional type). As core-only particles, these materials are promising candidates for PV applications, while as core/shell structures, they can find applications in displays, solid-state lighting, and bioimaging.

■ ASSOCIATED CONTENT

Supporting Information. XRD patterns, EDX spectra, bleach data for CIS core-only NCs, PL excitation data, and additional TEM images of CIS NCs. This material is available free of charge via the Internet at http://pubs.acs.org.

■ AUTHOR INFORMATION

Corresponding Author
klimov@lanl.gov

■ ACKNOWLEDGMENT

This material is based upon work within the Center for Advanced Solar Photophysics, an Energy Frontier Research Center funded by the U.S. Department of Energy (DOE), Office of Science, Office of Basic Energy Sciences (BES). J.M.P acknowledges support by the Chemical Sciences, Bioscience and Geosciences Division of BES, U.S. DOE. A.P. and B.P.K.. are Los Alamos National Laboratory Director's Postdoctoral Fellows. We thank Engang Fu for performing XRD.

■ REFERENCES

(1) (a) Allen, P. M.; Bawendi, M. G. *J. Am. Chem. Soc.* **2008,** *130,* 9240–9241. (b) Guo, Q.; Ford, G. M.; Hillhouse, H. W.; Agrawal, R. *Nano Lett.* **2009,** *9,* 3060–3065. (c) Guo, Q.; Kim, S. J.; Kar, M.; Shafarman, W. N.; Birkmire, R. W.; Stach, E. A.; Agrawal, R.; Hillhouse, H. W. *Nano Lett.* **2008,** *8,* 2982–2987. (d) Panthani, M. G.; Akhavan, V.; Goodfellow, B.; Schmidtke, J. P.; Dunn, L.; Dodabalapur, A.; Barbara, P. F.; Korgel, B. A. *J. Am. Chem. Soc.* **2008,** *130,* 16770–16777.

(2) Pons, T.; Pic, E.; Lequeux, N.; Cassette, E.; Bezdetnaya, L.; Guillemin, F.; Marchal, F.; Dubertret, B. *ACS Nano* **2010,** *4,* 2531–2538.

(3) Gurin, V. S. *Colloids Surf. A: Physicochem. Eng. Aspects* **1998,** *142,* 35–40.

(4) Li, B.; Xie, Y.; Huang, J. X.; Qian, Y. T. *Adv. Mater.* **1999,** *11,* 1456–1459.

(5) (a) Castro, S. L.; Bailey, S. G.; Raffaelle, R. P.; Banger, K. K.; Hepp, A. F. *J. Phys. Chem. B* **2004,** *108,* 12429–12435. (b) Castro, S. L.; Bailey, S. G.; Raffaelle, R. P.; Banger, K. K.; Hepp, A. F. *Chem. Mater.* **2003,** *15,* 3142–3147.

(6) Nairn, J. J.; Shapiro, P. J.; Twamley, B.; Pounds, T.; von Wandruszka, R.; Fletcher, T. R.; Williams, M.; Wang, C. M.; Norton, M. G. *Nano Lett.* **2006,** *6,* 1218–1223.

(7) (a) Norako, M. E.; Franzman, M. A.; Brutchey, R. L. *Chem. Mater.* **2009,** *21,* 4299–4304. (b) Xie, R. G.; Rutherford, M.; Peng, X. G. *J. Am. Chem. Soc.* **2009,** *131,* 5691–5697. (c) Zhong, H. Z.; Zhou, Y.; Ye, M. F.; He, Y. J.; Ye, J. P.; He, C.; Yang, C. H.; Li, Y. F. *Chem. Mater.* **2008,** *20,* 6434–6443.

(8) (a) Batabyal, S. K.; Tian, L.; Venkatram, N.; Ji, W.; Vittal, J. J. *J. Phys. Chem. C* **2009,** *113,* 15037–15042. (b) Koo, B.; Patel, R. N.; Korgel, B. A. *Chem. Mater.* **2009,** *21,* 1962–1966. (c) Nose, K.; Soma, Y.; Omata, T.; Otsuka-Yao-Matsuo, S. *Chem. Mater.* **2009,** *21,* 2607–2613. (d) Pan, D. C.; An, L. J.; Sun, Z. M.; Hou, W.; Yang, Y.; Yang, Z. Z.; Lu, Y. F. *J. Am. Chem. Soc.* **2008,** *130,* 5620–5621.

(9) Zhong, H.; Lo, S. S.; Mirkovic, T.; Li, Y.; Ding, Y.; Li, Y.; Scholes, G. D. *ACS Nano* **2010,** *4,* 5253–5262.

(10) Hishida, Y. J.; Toda, T.; Yoshie, T.; Yagi, K.; Yamaguchi, T.; Niina, T. *Appl. Phys. Lett.* **1994,** *64,* 3419–3421.

(11) Li, L.; Daou, T. J.; Texier, I.; Kim Chi, T. T.; Liem, N. Q.; Reiss, P. *Chem. Mater.* **2009,** *21,* 2422–2429.

(12) Alonso, M. I.; Wakita, K.; Pascual, J.; Garriga, M.; Yamamoto, N. *Phys. Rev. B* **2001,** 63.

(13) Klimov, V. I. *J. Phys. Chem. B* **2000,** *104,* 6112–6123.

(14) Crooker, S. A.; Barrick, T.; Hollingsworth, J. A.; Klimov, V. I. *Appl. Phys. Lett.* **2003,** *82,* 2793–2795.

(15) Zhong, H.; Zhou, Y.; Ye, M.; He, Y.; Ye, J.; He, C.; Yang, C.; Li, Y. *Chem. Mater.* **2008,** *20,* 6434–6443.

(16) Klimov, V. I.; McBranch, D. W.; Leatherdale, C. A.; Bawendi, M. G. *Phys. Rev. B* **1999,** *60,* 13740.

(17) (a) Hofhuis, J.; Schoonman, J.; Goossens, A. *J. Phys. Chem. C* **2008,** *112,* 15052–15059. (b) Rudigier, E.; Enzenhofer, T.; Scheer, R. *Thin Solid Films* **2005,** *480,* 327–331.

■ NOTE ADDED AFTER ASAP PUBLICATION

The caption for Figure 3 was corrected January 11, 2011.